JOURNAL OF GUIDANCE, CONTROL, AND DYNAMICS
Vol. 34, No. 4, July–August 2011

Kinematic Analysis and Control Design for a Nonplanar Multirotor Vehicle

Bill Crowther,* Alexander Lanzon,† Martin Maya-Gonzalez,‡ and David Langkamp§
University of Manchester, Manchester, England M13 9PL, United Kingdom

DOI: 10.2514/1.51186

A new class of nonplanar multirotor rotary vehicle is introduced that has the capability of independent control of both thrust and torque vectors in three dimensions. The vehicle configuration is based around the use of six thrust-producing rotors arranged in pairs on three separate reference planes. Variable thrust can be provided via fixed-pitch/variable-speed rotors or variable-pitch/fixed-speed rotors. The orientation of rotor reference planes affects the orthogonality of force and torque control, and it is shown how maneuverability can be traded with propulsive efficiency. The static mapping between force and torque control outputs and rotor inputs is derived from rotor geometry and a simple rotor aerodynamic model that does not include interference between rotors or fuselage drag and does not explicitly include induced-velocity effects. Controllers are synthesized for both position and attitude control, with acceptable stability demonstrated via Lyapunov analysis. Vehicle closed-loop dynamic response is investigated in simulation, and controller performance is shown to meet design requirements in the presence of unmodeled rotor inertia effects. Experimental results on a static test rig confirm that the simplified rotor aerodynamic modeling used for control synthesis is adequate for symmetric flight conditions around hover. A free-flying prototype has been flight-tested in hover, showing that practical vehicles are possible, accepting the fact that increased control capability comes at the expense of reduced payload and duration, compared with a conventional helicopter.

Nomenclature

$\mathbf{f}$	=	resultant force vector, $\in \Re^3$, N
$\mathbf{f}_i$, $\mathbf{F}_i$	=	force vector in three dimensions produced by the ith rotor, $\in \Re^3$, N
f_i	=	magnitude of force produced by the ith rotor, $\in \Re$, N
g	=	acceleration due to gravity, $\in \Re$ (9.8 m/s^2).
J	=	inertia tensor, $\in \Re^{3\times3}$, kg m^2
J_i	=	scalar moment of inertia of the ith rotor, $\in \Re$, kg m^2
J_r	=	scalar moment of inertia of a single rotor, $\in \Re$, kg m^2
$\hat{k}$	=	proportionality coefficient between rotor pitch angle θ_i and force f_i, $\in \Re$, N/rad
k_T	=	proportionality coefficient between the square of the rotor pitch angle θ_i^2 and rotor torque τ_i, $\in \Re$, Nm/rad^2
k_0	=	residual aerodynamic reaction drag experienced at zero rotor pitch angle, $\in \Re$, Nm
k_1	=	proportionality coefficient between the square of rotor spin speed, υ_i^2, and force f_i, $\in \Re$, Ns^2
k_2	=	proportionality coefficient between the square of rotor spin speed, υ_i^2, and rotor torque τ_i^2, $\in \Re$, Nms^2
l	=	rotor arm length, $\in \Re$, m
m	=	mass, $\in \Re$, kg
N_r	=	orientation matrix in $\Re^{3\times m}$ composed of the array of m vectors $\mathbf{n}_i$.
$\mathbf{n}_i$	=	unit vector parallel to the axis of the ith rotor, $\in \Re^3$.
$\mathbf{n}_x$, $\mathbf{n}_y$, $\mathbf{n}_z$	=	set of vectors equispaced in an angle α comprising a coordinate system for the characteristic force axes for a given configuration, $\in \Re^3$
$\mathbf{n}_{xyz}$	=	unit vector defining vehicle reference-plane normal, $\in \Re^3$.
$\mathbf{q}$	=	quaternion vector, $\in \Re^4$.
R	=	rotational matrix mapping vectors read in body axes to the same vector read in Earth axes, $\in \Re^{3\times3}$.
$\mathbf{r}$	=	position vector, $\in \Re^3$, m
$\mathbf{T}_i$	=	torque vector generated by the ith rotor, $\in \Re^3$, Nm
$\mathbf{t}$	=	torque vector, $\in \Re^3$, Nm
$\mathbf{t}_i$	=	reaction torque produced by the ith rotor in body axes, $\in \Re^3$, Nm
t_{x_m}, t_{y_m}, t_{z_m}	=	vectors representing the principal torques in body axes, $\in \Re^3$, Nm
V	=	Lyapunov candidate function, $\in \Re$, $V \geq 0$.
υ_i,ω_i	=	angular speed of the ith rotor, $\in \Re$, rad/s
X_r	=	position matrix in $\Re^{3\times m}$ composed of the array of m vectors $\mathbf{x}_i$, m
$\mathbf{x}$,$\mathbf{y}$, $\mathbf{z}$	=	set of vectors defining the characteristic axis system, $\in \Re^3$.
$\mathbf{x}_i$	=	position vector of the ith rotor, $\in \Re^3$, m
$\mathbf{x}_m$, $\mathbf{y}_m$, $\mathbf{z}_m$	=	set of vectors defining the principal torque axes in body axes, $\in \Re^3$.
α	=	angle between the principal forces, rad
β	=	angle between the principal moments, rad
θ_i	=	collective pitch angle of the ith rotor, rad
τ_i	=	magnitude of the reaction torque produced by the ith rotor, parallel to the $\mathbf{n}_i$ vector, $\in \Re$, Nm
ϕ	=	disk plane angle, rad
$\boldsymbol{\omega}$	=	angular velocity vector, $\in \Re^3$, rad/s

Subscripts

b	=	vectors defined in body axes.

Received 17 June 2010; revision received 2 February 2011; accepted for publication 5 February 2011.

*School of Mechanical, Aerospace and Civil Engineering, Room C27, George Begg Building; w.j.crowther@manchester.ac.uk.

†Control Systems Centre, School of Electrical and Electronic Engineering, Sackville Street Building; Alexander.Lanzon@manchester.ac.uk.

‡Control Systems Centre, School of Electrical and Electronic Engineering, Sackville Street Building; Martin.MayaGonzalez@postgrad.manchester.ac.uk (Corresponding Author).

§School of Mechanical, Aerospace and Civil Engineering, Room C27, George Begg Building; David.Langkamp@postgrad.manchester.ac.uk.

0 = vectors defined in Earth axes.
0123 = selected ordered elements

Superscript

d = Desired (or reference) signals.

I. Introduction

THIS paper introduces a class of nonplanar rotary-wing vehicle in which both the vehicle thrust and torque vectors can be arbitrarily orientated with respect to the vehicle body axes under quiescent conditions [1]. This capability enables fully independent control of both vehicle position and orientation in three-dimensional space, at least during hover or slow forward flight (within the saturation limits of the actuators). Provision of arbitrary pointing of torque and thrust vectors on a vehicle is, in itself, relatively commonplace: for example, many vehicles that use buoyancy as a means of weight support (such as underwater vehicles or lighter-than-air vehicles) have this capability, as do vehicles that operate in low-gravity environments (such as satellites). The key contribution of the work in this paper is the elucidation of a practical rotary-wing vehicle solution that meets the independent thrust and torque-pointing criteria in which the control actuators also provide the weight support function of the vehicle. The benefits of improved control authority inevitably come at the expense of increased vehicle mass, and any future application will have to consider the tradeoff between vehicle performance (duration, range, and payload) and level of independent control authority. Furthermore, the current work does not consider aerodynamic interference effects between rotors or fuselage drag, and hence the applicability of the concept to control in forward flight and under wind disturbances is, as yet, unproven.

Since there are many multirotor rotary-wing configurations in existence, it is important to clearly define the vehicle class to which the work in the present paper contributes. The first distinction is that for the vehicle class of interest the orientation of the planes of rotation of individual rotors on the vehicle is fixed with respect to the vehicle body axes. Thus, vehicles with variable-orientation rotors (such as tiltrotor craft) and designs with rotor cyclic pitch control (such as conventional single- and twin-rotor helicopters) are excluded from the class of interest. This distinction is noteworthy in that there is significant mechanical complexity, and hence weight and cost, associated with tiltrotor designs and the provision of a swashplate for cyclic control. The second distinction is that the vehicle must possess six or more rotors arranged on at least three different planes, capable of delivering thrust at a range of magnitudes for control actuation purposes. The requirement for six or more rotors on three different planes stems from the need to control all six degrees of freedom and will be covered further in the vehicle configuration discussion in Sec. II. With regard to the manner in which the thrust of the rotor is varied, the vehicle class of interest includes both fixed-rotor-pitch/variable-rotor-speed designs and fixed-speed/variable-(collective)-pitch designs. The examples and case study considered in this paper are all based on configurations with six rotors of equal size arranged in a number of different geometric arrangements that satisfy the independent thrust and torque-vectoring requirements. For ease of reference in this paper, vehicles corresponding to the class described above will be referred to as hexrotor vehicles, with additional information added to describe the geometric arrangement of rotors for which this is appropriate.

A photograph of a prototype hexrotor vehicle developed as part of the present work is shown in Fig. 1a. This vehicle is powered by six electric motors driving six fixed-pitch propellers and is an example of an orthogonal edge-centered type-I configuration according to the taxonomy defined in Sec. II. A prototype of the vehicle was successfully flown in hover and slow forward flight using manual command of attitude rates and thrust magnitude in November 2009; see Sec. VIII.E for brief further details of the flight test.

An envisaged mission for a hexrotorlike vehicle that makes use of its unique properties is shown in Fig. 2. The work in this paper contributes toward development of the overall vehicle configuration and controller design for hover and slow forward flight. It is recognized that significant additional work is required to develop additional controllers for the ground contact phase of the mission shown and supervisory strategy for switching between air and ground controllers. Note that the hexrotor vehicle has some passing resemblance with the rotochute concept [2], in that with an appropriate outer frame it can support a ground reaction at arbitrary attitude. However, beyond this, there is very little in common from a vehicle design and control perspective.

Although the concept of a nonplanar multirotor vehicle is novel, there is a significant body of knowledge on planar multirotor vehicles, in particular quadrotors, that is relevant, e.g., work by Hoffmann et al. [3], Waslander et al. [4], Valavanis [5], Bouabdallah et al. [6], Stepaniak et al. [7,8], and Pounds et al. [9–11]. The main points of relevance are that the typical rotor disk loading and Reynolds numbers are similar, both use closely spaced rotors meaning rotor interference effects may be important, and the fuselage structures are similar, meaning that fuselage aerodynamic effects are likely to be similar. As a point of difference it is noted that planar vehicles can make use of translational lift, whereas this is likely to cause interference in nonplanar vehicles. The overall aerodynamics of nonplanar multirotor vehicles with arbitrary thrust direction is clearly more complex than for planar vehicles and the present work has had to make a number of simplifying assumptions to move the design problem forward. As a starting point in keeping with typical practice used in the quadrotor literature, the effect of the rotor wakes on the fuselage are ignored and the airframe drag is assumed to be insignificant in low-speed, near-hover flight conditions.

The structure of this paper is as follows. Section II gives a kinematic analysis of multirotor vehicle configurations. Section III presents the forward and inverse statics models for the hexrotor

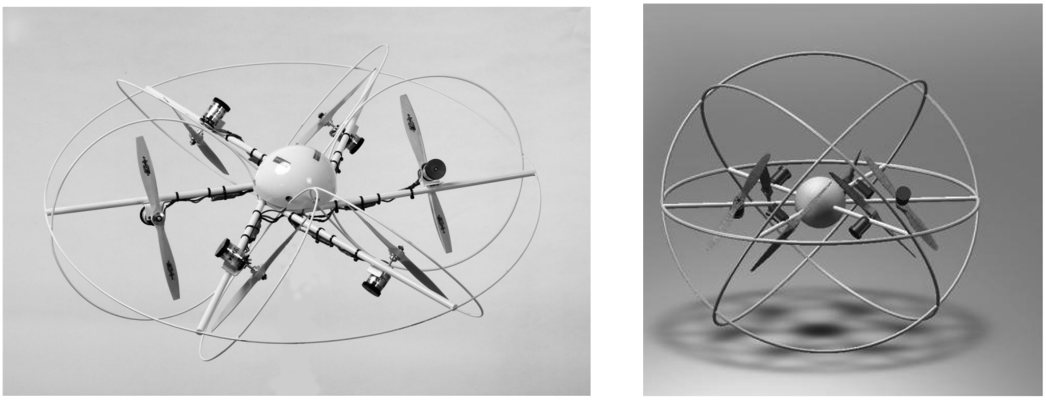

a) Hexrotor prototype. Rotor diameter 38cm, overall vehicle mass 5.5kg, hover duration 5 minutes

b) CAD illustration of a hexrotor vehicle in a rolling frame

Fig. 1 Orthogonal face-centered hexrotor implementations.

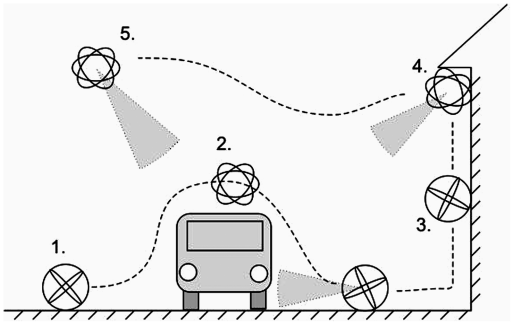

Fig. 2 Concept of operation for a hexrotor vehicle. 1: roll to target, 2: free-flight translation, 3: roll up vertical wall, 4: press and stare, and 5: free hover.

vehicle. Section IV focuses on the dynamics model of the hexrotor vehicle. Section V describes the control strategy adopted. Stability analysis for the attitude control system is presented in Sec. VI. Relations between quaternion attitude rates and angular velocity vectors are discussed in Sec. VII. Section VIII presents experimental results and some simulation results, and the conclusions are presented in Sec. IX.

II. Vehicle Configuration Design

This section provides an analysis of the force and torque characteristics of a generic multirotor helicopter based on the geometric arrangement of rotors, leading to a general result that provides theoretical proof for the existence of a class of six rotor vehicles with independent control of both force and torque. The analysis assumes that orientations of the rotor disks are fixed with respect to the body and that the rotor aerodynamic force is normal to the plane of rotation of the rotor. The former condition implies a rigid rotor without cyclic control and the latter conditions implies that the analysis is limited flight conditions around hover.

A. Generalized Force and Torque Equations for Multirotor Vehicles

Consider a generic multirotor vehicle with m rotor disks. Let the positions of the m rotor disks with respect to the vehicle body axes be defined by a $3 \times m$ matrix X_r, composed of position column vectors $\mathbf{x}_i \in \Re^3$, where $i = 1, 2, \ldots, m$, and let the orientations of these disks be defined by $3 \times m$ matrix N_r, composed of rotor normal unit vectors $\mathbf{n}_i \in \Re^3$, where $i = 1, 2, \ldots, m$ are in the vehicles body axes. Assume each rotor spins with angular velocity ω_i, where $i = 1, 2, \ldots, m$, with positive defined as anticlockwise about the rotor normal $\mathbf{n}_i$. Each rotor provides a force in the rotor normal direction $\mathbf{n}_i$. The magnitude of the rotor forces can be varied by either independent or combined changes in the rotor collective pitch angle and rotor speed, and the forces can be positive or negative. Assuming the orientation of the rotor normal cannot be varied, the force of the ith rotor can be expressed as the normal vector $\mathbf{n}_i$ multiplied by the scalar magnitude of force f_i [12]:

$$\mathbf{F}_i = \mathbf{n}_i f_i \tag{1}$$

Rotor forces produce a torque about the vehicle origin, associated with the cross product of the rotor force $\mathbf{F}_i$ and the respective position vector $\mathbf{x}_i$. Each rotor additionally produces an aerodynamic reaction torque with magnitude τ_i about the axis of rotation $\mathbf{n}_i$, with a sign opposite to that of the direction of rotation. The vehicle also experiences a torque $J_i\dot{\omega}_i$, associated with the rate of change of angular momentum of each disk [12]. The torque description is summarized in the following expression:

$$\mathbf{T}_i = (\mathbf{x}_i \times \mathbf{n}_i) f_i - \mathbf{n}_i \tau_i - \mathbf{n}_i J_i \dot{\omega}_i \tag{2}$$

The generalized expressions for force for a multirotor vehicle can then be written down as

$$\mathbf{F} = N_r f \tag{3}$$

and the generalized equation for torque is written as

$$\mathbf{T} = (X_r \times N_r) f - N_r(\tau + J\dot{\omega}) \tag{4}$$

where the forces, torques, moments of inertia, and rotational speed in the above two equations are, respectively, given by

$$f = \begin{bmatrix} f_1 \\ f_2 \\ \vdots \\ f_m \end{bmatrix}, \quad \tau = \begin{bmatrix} \tau_1 \\ \tau_2 \\ \vdots \\ \tau_m \end{bmatrix}, \quad J = \begin{bmatrix} J_1 & 0 & 0 & 0 \\ 0 & J_2 & 0 & 0 \\ 0 & 0 & \ddots & 0 \\ 0 & 0 & 0 & J_m \end{bmatrix}$$
$$\omega = \begin{bmatrix} \omega_1 \\ \omega_2 \\ \vdots \\ \omega_m \end{bmatrix} \tag{5}$$

The cross product $X_r \times N_r$ is a $3 \times m$ matrix composed of an array of vectors $(\mathbf{x}_i \times \mathbf{n}_i)$ and is calculated as the cross product of position and normal direction vectors.

B. Hexrotor Vehicles with Orthogonal Disk Planes

For a six rotor vehicle there are a large number of ways in which the rotors can be positioned and orientated and engineering judgment is required to identify solutions with the greatest degree of practicality. First, preferred arrangements use paired planar rotors with opposite spin directions to achieve as near as possible a vehicle with zero net angular momentum. Second, it is assumed that the three rotor pairs exist on three characteristic planes that pass through the origin of the vehicle axes and whose normals define three equispaced characteristic axes.

Figure 3 shows three different arrangements of a hexrotor vehicle based on the use of three pairs of rotors placed on three orthogonal reference planes. It is instructive to divide the configurations into what we define as face-centered and edge-centered designs, depending on the location of the rotor disks relative to the characteristic axes. Furthermore, for the face-centered configuration there are two distinctly different arrangements identified as type I and type II. With the type-I arrangement the rotors' centers exist on a single plane defined as the vehicle reference plane that passes through the center of the vehicle. For the type-II arrangement, the disk centers lie on two different parallel planes that pass above and below the center of the vehicle. The edge-centered configuration can only exist in one arrangement. The following provides an analysis of a hexrotor with a face-centered type-I configuration. The position and orientation matrices of the rotors for this configuration are given by

$$X_r = a \begin{bmatrix} 1 & 0 & -1 & -1 & 0 & 1 \\ 0 & 1 & 1 & 0 & -1 & -1 \\ -1 & -1 & 0 & 1 & 1 & 0 \end{bmatrix} \tag{6}$$

$$N_r = \begin{bmatrix} 0 & 1 & 0 & 0 & 1 & 0 \\ 1 & 0 & 0 & 1 & 0 & 0 \\ 0 & 0 & 1 & 0 & 0 & 1 \end{bmatrix} \tag{7}$$

Substitution into the force and torque equations (3) and (4) gives

$$\mathbf{F} = \begin{bmatrix} f_2 + f_5 \\ f_1 + f_4 \\ f_3 + f_6 \end{bmatrix} \tag{8}$$

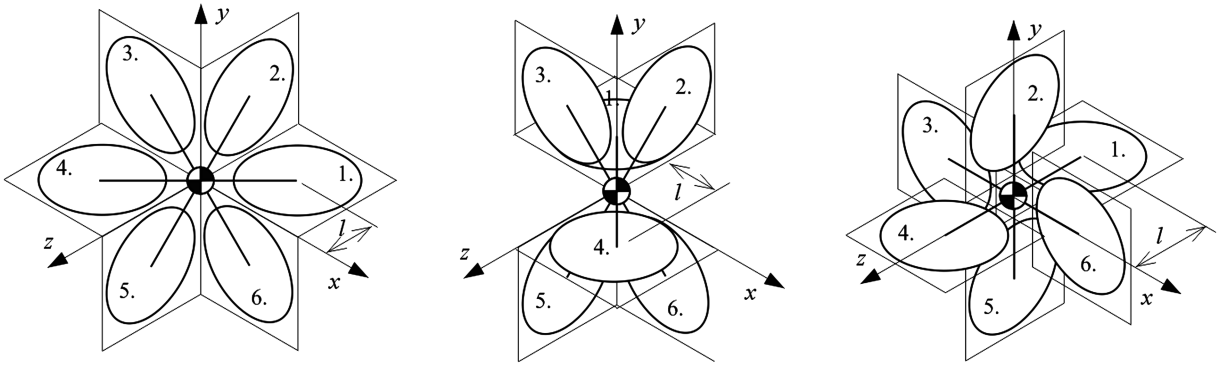

a) Face-centered **b) Edge-centered**

Fig. 3 Geometric definition of rotor arrangements for an orthogonal hexrotor vehicle.

$$\mathbf{T} = \begin{bmatrix} -\tau_2 - \tau_5 + a(f_1 - f_4 + f_3 - f_6) \\ -\tau_1 - \tau_4 + a(f_5 - f_2 + f_3 - f_6) \\ -\tau_3 - \tau_6 + a(f_1 - f_4 + f_5 - f_2) \end{bmatrix} \tag{9}$$

It can be seen from Eqs. (8) and (9) that a hexrotor vehicle is able to produce control force and moment components in all three (orthogonal) dimensions, meaning that the thrust and torque vectors can, in principle, be arbitrarily orientated in three-dimensional space. A more formal mathematical treatment of this statement is provided in Sec. III as part of the aerodynamic modeling. Equations (8) and (9) also show that there is a degree of mechanical robustness in the provision of actuation, because there is redundancy in the torque sources, such that one rotor can fail without compromising attitude control. Note that for orthogonal rotor reference planes with all rotors operational, the available components of force will be orthogonal. However, as a result of geometric differences, the components of torque for the face-centered arrangement are not orthogonal, whereas the torque components for the edge-centered arrangement are orthogonal.

C. Hexrotor Vehicles with Nonorthogonal Disk Planes

The preceding analysis has considered hexrotor configurations based on orthogonal disk reference planes. The following now considers the more general case in which the disk reference planes are nonorthogonal. This is important, because the degree of orthogonality between the disk reference planes allows a designer to make tradeoffs between the overall propulsive efficiency of the vehicle (maximized when the disk reference planes are coplanar) and the degree to which orthogonality of force and torque control is required for a particular application. The following analysis is specifically applied to the face-centered planar configuration from Fig. 3a; however, the same broad outcomes are applicable to the other hexrotor configurations of interest.

Let three unit vectors $\mathbf{n}_x$, $\mathbf{n}_y$, and $\mathbf{n}_z$ from Fig. 4b, expressed in three-dimensional space and equispaced by an angle α, define a coordinate system for the characteristic force axes of a multirotor vehicle with rotor configuration N_r. Angle α is, by definition, given by

$$\alpha = \arccos(\mathbf{n}_x \cdot \mathbf{n}_y) = \arccos(\mathbf{n}_y \cdot \mathbf{n}_z) = \arccos(\mathbf{n}_z \cdot \mathbf{n}_x) \tag{10}$$

where the centered dot represents the dot product for vectors.

Let the lines of intersection between the three planes defined by $\mathbf{n}_x$, $\mathbf{n}_y$, $\mathbf{n}_z$, and the vehicle origin define a characteristic axis system **xyz**. The basis vectors for the **xyz** characteristic axis system are, by definition,

$$\mathbf{x} = \mathbf{n}_y \times \mathbf{n}_z, \qquad \mathbf{y} = \mathbf{n}_z \times \mathbf{n}_x, \qquad \mathbf{z} = \mathbf{n}_x \times \mathbf{n}_y \tag{11}$$

For the special orthogonal case when $\alpha = \pi/2$, corresponding to the configuration shown in Fig. 3a, the **xyz** characteristic axis systems are

$$\mathbf{x} = \mathbf{n}_x, \qquad \mathbf{y} = \mathbf{n}_y, \qquad \mathbf{z} = \mathbf{n}_z \tag{12}$$

Using the basis vectors from the axis system **xyz**, the vehicle reference plane is defined by the unit normal vector given by

$$\mathbf{n}_{xyz} = \frac{\mathbf{x} + \mathbf{y} + \mathbf{z}}{\|\mathbf{x} + \mathbf{y} + \mathbf{z}\|}$$

A derived reference angle ϕ referred to as the disk plane angle represents the angle between the rotor planes and the vehicle reference plane. The degree of orthogonality between the characteristic force axes can be shown to be equal to the disk plane angle, calculated as the following dot product:

$$\phi = \arccos(\mathbf{n}_x \cdot \mathbf{n}_{xyz}) = \arccos(\mathbf{n}_y \cdot \mathbf{n}_{xyz}) = \arccos(\mathbf{n}_z \cdot \mathbf{n}_{xyz}) \tag{13}$$

The relationship between the disk plane angle and the angle α between the characteristic force axes is defined by geometry and can be shown to be equal to

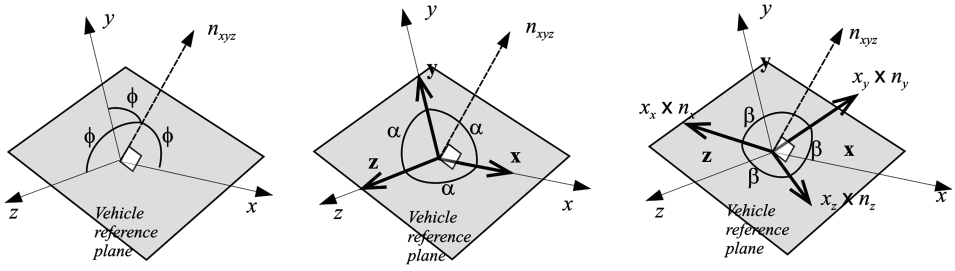

a) Disc plane angle, ϕ **b) Force orthogonality, α** **c) Torque orthogonality, β**

Fig. 4 Geometric definition of disk plane angle and force and torque orthogonality.

$$\alpha = \arccos(-\tfrac{1}{2}\sin^2\phi + \cos^2\phi) \tag{14}$$

In a similar way, it can be shown that the angle β between the characteristic torque axes is defined by

$$\beta = \pi - \arccos(\tfrac{1}{2}\cos^2\phi - \sin^2\phi) \tag{15}$$

Note that angle β in Fig. 4c is based on the principal moments obtained from the cross product of rotor forces and position and does not take into account the aerodynamic and inertial torques produced by the rotors as defined by Eq. (4). As such, it is only a partial measure of orthogonality of the torque principal axes. However, since the force-distance cross product term will typically be an order of magnitude greater than the aerodynamic and dynamic torques, it provides a useful metric to guide choice of the disk plane angle based on specified operational requirements.

Orthogonality of control force and torque components is advantageous, because it minimizes the energy (or effort) required to achieve a given force or torque vector. For highly nonorthogonal systems, i.e., cases in which α and/or β are significantly different from 90 deg, it is possible that significant energy or effort is used by one or more than one rotor to cancel out competing force or torque components. Such a highly nonorthogonal implementation might also suffer from reduced control authority, because rotor thrust saturation limits are being reached at lower overall body-axis force levels.

The relationships given by Eqs. (14) and (15) are shown in Fig. 5. This plot identifies the tradeoffs between orthogonality of characteristic force and torque axes and the disk plane angle. To achieve efficiency in the hover mode, the disk plane angle φ should tend toward zero such that all the rotors are producing a force in the same direction. However, this would lead to a fully planar structure in which the characteristic force axes are aligned ($\phi = 0$), i.e., a control force can only be produced in a direction normal to the vehicle reference plane. This arrangement is similar to a quadrotor, from an actuation point of view. For a disk angle of 45 deg, the orthogonality angles for the force and torque axes are both equal to 75.5 deg. This provides a vehicle with a reasonably efficient hover and thrust and torque orthogonality reasonably close to the ideal of 90 deg for efficient actuation. However, the highest authority and most energy-efficient thrust vectoring occurs when the characteristic force axes are orthogonal ($\alpha = 90$ deg). For this case, the disk plane angle in Fig. 5 is 54.7 deg and the angle between characteristic torque axes is 60 deg.

D. Basic Performance Comparison Between Planar and Nonplanar Multirotor Vehicles

This section provides a brief analysis of the performance implications of using nonplanar rotary-wing vehicles such as the hexrotor. It is a given that provision of lift equal to or greater than weight at any attitude will come at the expense of increased overall propulsion system mass, compared with a vehicle that needs only meet this requirement at one attitude. Furthermore, it is a given that the propulsive efficiency of a nonplanar multirotor vehicle at any given attitude will be less than that of an equivalent planar vehicle with rotor plane normal to the direction of thrust. In engineering terms, the first issue relates to the sizing of the installed power systems and the second issue relates to sizing of the stored-energy system (battery).

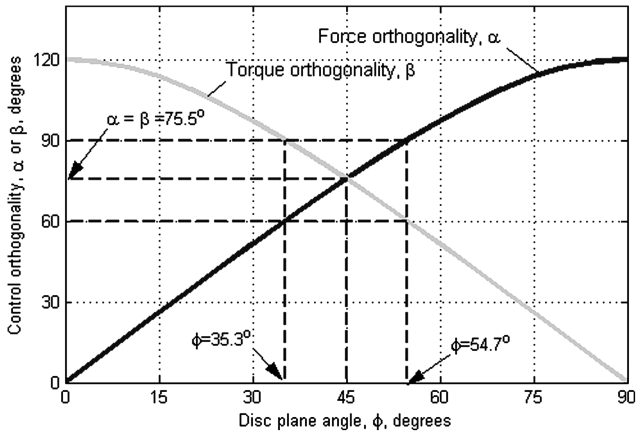

Fig. 5 Effect of disk plane angle on orthogonality of forces and torques for a face-centered hexrotor configuration.

To address the issue of increased propulsion system mass for nonplanar vehicles, consider the case of an orthogonal hexrotor configuration in steady hover. The most demanding hover attitudes for this orthogonal configuration will be those where the whole weight of the vehicle is supported on a single pair of rotors, with the other two pairs of rotors making a contribution of zero to weight support. Thus, the critical design case for sizing the propulsion system is that a single pair of rotors needs to provide sufficient thrust to support the weight of the vehicle, including two additional pairs of deadweight propulsion units that are not contributing to thrust. This means that power rating of individual propulsion units might be up to 3 times higher than it would be for an equivalent planar vehicle. As a practical example, the propulsion unit mass in terms of propeller, motor, and speed controller for a quadrotor electric rotary-wing vehicle will be of the order of 30–35% of the overall mass of the vehicle [5]. For the prototype hexrotor vehicle developed in this work the propulsion unit mass is 55% of the overall mass.

With regard to reduced propulsive efficiency of nonplanar vehicles, there will always be an element of rotors working against each other at any attitude and hence reduced efficiency compared with planar designs. A simple analysis based simply on resolution of forces gives that for an orthogonal hexrotor configuration generating a force normal to the vehicle reference plane, the sum of the force magnitudes from each of the rotors will be $1/\cos(54.7\,\text{deg}) = 1.7$ times the force normal to the reference plane.

III. Statics Model

The kinematic analysis relates the connection between the available actuation and the configuration of the rotor system. The paper now focuses on calculating the system actuations, given the required forces and torques; an inverse problem of the first kind [13]. To start the analysis, the direct problem, or the calculation of forces and torques generated by the system actuators, is tackled first. The analysis uses a rotor model based on linear aerodynamics [12,13]. The effects of induced velocity and interference between rotors are not included. Given the limitations in the physics, the model is applicable for flight conditions around hover only and will be of limited accuracy at flight conditions where wakes from one rotor are ingested by other rotors. A more sophisticated analysis is required for translating flight and is considered to be beyond the scope of this paper.

The synthesis of the force and moment vectors depends on understanding the effects of the vehicle force and torque equations (8) and (9). The geometric interpretation of those vectors for an orthogonal face-centered hexrotor configuration is shown Fig. 6. Recall that for this configuration, the principal force axes form an orthogonal coordinate system. It is analytically convenient to make the vehicle body-axis coordinate system coincident with this coordinate system; hence, the principal force axes are now labeled $\mathbf{x}_b$, $\mathbf{y}_b$, and $\mathbf{z}_b$.

In Fig. 6a, the first and fourth rotors have opposite reaction torques $\mathbf{t}_1$ and $\mathbf{t}_4$ and opposite spin directions. The same applies to the second and fifth rotors and their corresponding reaction torques $\mathbf{t}_2$ and $\mathbf{t}_5$, as well as the third and sixth with reaction torques $\mathbf{t}_3$ and $\mathbf{t}_6$. Figure 6b shows that thrusts $\mathbf{f}_1$ and $\mathbf{f}_4$ are generated by the first and fourth rotors, operating at a distance of l from the intersection of the vehicle with axis $\mathbf{y}_b$ and are pointing in the same direction. The same applies to the forces $\mathbf{f}_2$ and $\mathbf{f}_5$, with axes $\mathbf{x}_b$, associated with the second and fifth rotors and with $\mathbf{f}_3$ and $\mathbf{f}_6$, with axes $\mathbf{z}_b$, associated with the third and sixth rotors.

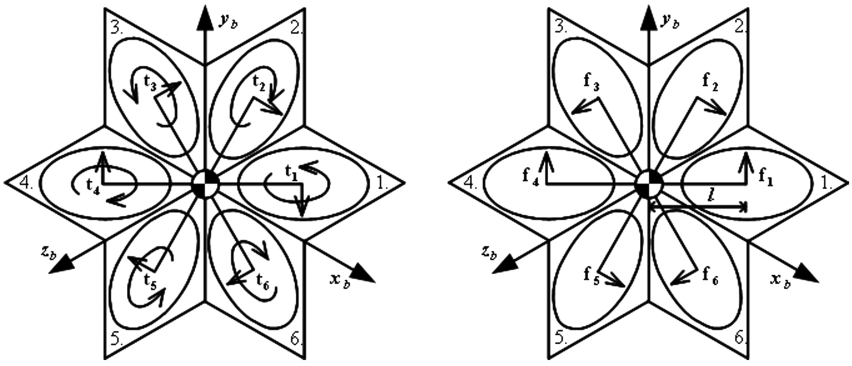

a) Rotor spin directions and drag torques **b) Rotor forces**

Fig. 6 Definition of rotor spin directions, drag torques, and forces.

A. Propulsion via Constant-Speed/Variable-Pitch Rotors

Provision of variable-pitch rotors enables production of forces in the positive and negative directions. The thruster consists of a rotor i producing a perpendicular force that is function of the collective pitch angle θ_i. In this case θ_i is the controllable variable. The thrust is described by the force function for propellers [12]:

$$f_i = \hat{k}\theta_i \tag{16}$$

where $\hat{k}$ is a scalar constant coefficient of proportionality that relates rotor pitch angle to force as in (16) and has units of newtons/radian. Note that the constant $\hat{k}$ is dependent on the rotor geometry and is specific to the hover operating conditions. Referring to Fig. 6b, the force equation in body axes is obtained by substituting the rotor position equation (7) into the net force equation (3):

$$\mathbf{f}_b = N_r f = \begin{pmatrix} 0 & 1 & 0 & 0 & 1 & 0 \\ 1 & 0 & 0 & 1 & 0 & 0 \\ 0 & 0 & 1 & 0 & 0 & 1 \end{pmatrix} \begin{pmatrix} f_1 \\ f_2 \\ f_3 \\ f_4 \\ f_5 \\ f_6 \end{pmatrix} \tag{17}$$

To complete the direct problem, the command pitch angles in Eq. (16) are substituted into the force equation (17) and are then converted into the Earth axes using $\mathbf{r}_0 = R\mathbf{r}_b$, which is the same frame in which the translational dynamics are defined, to give the net resultant force on the vehicle:

$$\mathbf{f}_0 = RN_r f = \hat{k}R \begin{pmatrix} 0 & 1 & 0 & 0 & 1 & 0 \\ 1 & 0 & 0 & 1 & 0 & 0 \\ 0 & 0 & 1 & 0 & 0 & 1 \end{pmatrix} \begin{pmatrix} \theta_1 \\ \theta_2 \\ \theta_3 \\ \theta_4 \\ \theta_5 \\ \theta_6 \end{pmatrix} \tag{18}$$

Figure 7 shows the differential force moments (i.e., the total moment minus the aerodynamic drag torques) about the principal torque axes $\mathbf{x}_m$, $\mathbf{y}_m$, and $\mathbf{z}_m$ drawn in body axes $\mathbf{x}_b$, $\mathbf{y}_b$, and $\mathbf{z}_b$. Using the nomenclature in Fig. 6b the so-called differential force moments are given by

$$t_{x_m} = l(f_3 - f_6) \tag{19}$$

$$t_{y_m} = l(f_5 - f_2) \tag{20}$$

$$t_{z_m} = l(f_1 - f_4) \tag{21}$$

These moments are expressed in body axes using the matrix R_{mb}. Next, the torque direct problem is solved by substituting the command mapping of force equation (16) into the differential moments:

$$\mathbf{t}_{b_d} = R_{mb} \begin{pmatrix} t_{x_m} \\ t_{y_m} \\ t_{z_m} \end{pmatrix} = \begin{pmatrix} \frac{1}{\sqrt{2}} & 0 & \frac{1}{\sqrt{2}} \\ \frac{1}{\sqrt{2}} & \frac{1}{\sqrt{2}} & 0 \\ 0 & \frac{1}{\sqrt{2}} & \frac{1}{\sqrt{2}} \end{pmatrix} \begin{pmatrix} \hat{k}l(\theta_3 - \theta_6) \\ \hat{k}l(\theta_5 - \theta_2) \\ \hat{k}l(\theta_1 - \theta_4) \end{pmatrix} \tag{22}$$

From simple propeller theory [12] the propulsive reaction torque as a function of pitch angle θ_i for a given rotor i in hover is given by

$$\tau_i = k_0 + k_T \theta_i^2 \tag{23}$$

where k_T is a scalar constant coefficient of proportionality that relates rotor pitch angle to aerodynamic reaction drag experienced by the rotor, as given in Eq. (23), and hence has units of $\mathrm{Nm/rad^2}$. The constant k_0 is the residual aerodynamic reaction drag experienced at zero rotor pitch angle with units of newton meters [12]. Although Eq. (23) represents a simplification, experimental data suggests that in hover conditions the torque equation is mainly driven by the constant and quadratic terms, and hence Eq. (23) is suitable for this purpose.

The reaction torque generated by the rotors is calculated as a function of the pitch angle θ_i by replacing the individual reaction torque equation (23) into the total torque equation (4), considering the normal rotor axis stated in the matrix N_r from Eq. (7):

$$\mathbf{t}_{b_r} = k_T \begin{pmatrix} \theta_2^2 - \theta_5^2 \\ \theta_4^2 - \theta_1^2 \\ \theta_6^2 - \theta_3^2 \end{pmatrix} \tag{24}$$

Combining both differential $\mathbf{t}_{b_d}$ torques [Eq. (22)] and reaction torques $\mathbf{t}_{b_r}$ [Eq. (24)] gives the net torque $\mathbf{t}_b$ in the body axes:

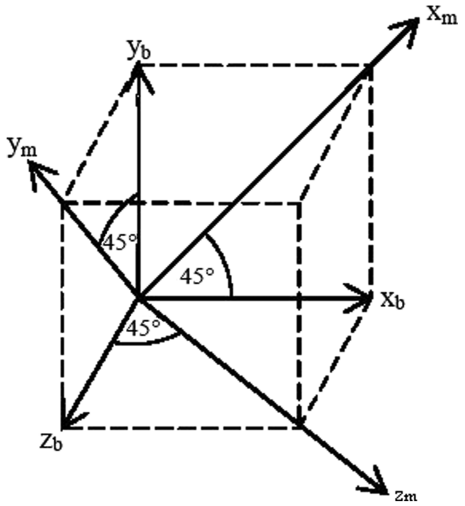

Fig. 7 Relationship between the principal torque axes and vehicle body axes for an orthogonal face-centered hexrotor.

$$\mathbf{t}_b = \left[\frac{\hat{k}l}{\sqrt{2}} \begin{pmatrix} 1 & 0 & 1 & -1 & 0 & -1 \\ 0 & -1 & 1 & 0 & 1 & -1 \\ 1 & -1 & 0 & -1 & 1 & 0 \end{pmatrix} \begin{pmatrix} \theta_1 \\ \theta_2 \\ \theta_3 \\ \theta_4 \\ \theta_5 \\ \theta_6 \end{pmatrix} + k_T \begin{pmatrix} 0 & 1 & 0 & 0 & -1 & 0 \\ -1 & 0 & 0 & 1 & 0 & 0 \\ 0 & 0 & -1 & 0 & 0 & 1 \end{pmatrix} \begin{pmatrix} \theta_1^2 \\ \theta_2^2 \\ \theta_3^2 \\ \theta_4^2 \\ \theta_5^2 \\ \theta_6^2 \end{pmatrix} \right] \tag{25}$$

From the direct problem solution, the forces and torques acting on the vehicle are given by the following composite vector:

$$\begin{pmatrix} \mathbf{f}_0 \\ \mathbf{t}_b \end{pmatrix} = \begin{pmatrix} R & 0 \\ 0 & I \end{pmatrix} \left[\begin{pmatrix} P & P \\ Q & -Q \end{pmatrix} \begin{pmatrix} \theta_1 \\ \theta_2 \\ \theta_3 \\ \theta_4 \\ \theta_5 \\ \theta_6 \end{pmatrix} + \begin{pmatrix} 0 & 0 \\ S & -S \end{pmatrix} \begin{pmatrix} \theta_1^2 \\ \theta_2^2 \\ \theta_3^2 \\ \theta_4^2 \\ \theta_5^2 \\ \theta_6^2 \end{pmatrix} \right] \tag{26}$$

where the matrices P, Q, and S are, respectively, given by

$$P = \hat{k} \begin{pmatrix} 0 & 1 & 0 \\ 1 & 0 & 0 \\ 0 & 0 & 1 \end{pmatrix} \tag{27}$$

$$Q = \frac{\hat{k}l}{\sqrt{2}} \begin{pmatrix} 1 & 0 & 1 \\ 0 & -1 & 1 \\ 1 & -1 & 0 \end{pmatrix} \tag{28}$$

$$S = k_T \begin{pmatrix} 0 & 1 & 0 \\ -1 & 0 & 0 \\ 0 & 0 & -1 \end{pmatrix} \tag{29}$$

To solve an inverse problem of the first kind, it is necessary to map the commanded pitch angle θ_i into net force and torque requirements. Initially, matrix inversion is carried out to obtain the following matrix equation:

$$\frac{1}{2} \begin{pmatrix} I & I \\ I & -I \end{pmatrix} \begin{pmatrix} P^{-1}R^T & 0 \\ 0 & Q^{-1} \end{pmatrix} \begin{pmatrix} \mathbf{f}_0 \\ \mathbf{t}_b \end{pmatrix} = \begin{pmatrix} \theta_1 \\ \theta_2 \\ \theta_3 \\ \theta_4 \\ \theta_5 \\ \theta_6 \end{pmatrix} + \frac{1}{2} \begin{pmatrix} Q^{-1}S \\ -Q^{-1}S \end{pmatrix} (I \quad -I) \begin{pmatrix} \theta_1^2 \\ \theta_2^2 \\ \theta_3^2 \\ \theta_4^2 \\ \theta_5^2 \\ \theta_6^2 \end{pmatrix} \tag{30}$$

Assume that the following net force $\mathbf{f}_0 = [\, f_{0_1} \quad f_{0_2} \quad f_{0_3} \,]^T$ and torque $\mathbf{t}_b = [\, t_{b_1} \quad t_{b_2} \quad t_{b_3} \,]^T$ are required. To make the calculation easier, the left side of Eq. (30) is defined as the requirement vector $[\, u_1 \quad u_2 \quad u_3 \quad u_4 \quad u_5 \quad u_6 \,]^T$:

$$\begin{pmatrix} u_1 \\ u_2 \\ u_3 \\ u_4 \\ u_5 \\ u_6 \end{pmatrix} = \frac{1}{2} \begin{pmatrix} I & I \\ I & -I \end{pmatrix} \begin{pmatrix} P^{-1}R^T & 0 \\ 0 & Q^{-1} \end{pmatrix} \begin{pmatrix} f_{0_1} \\ f_{0_2} \\ f_{0_3} \\ t_{b_1} \\ t_{b_2} \\ t_{b_3} \end{pmatrix} \tag{31}$$

When substituted into the right side of Eq. (30), we are left with a matrix whose only unknown values are the pitch angles θ_i:

$$\begin{pmatrix} u_1 \\ u_2 \\ u_3 \\ u_4 \\ u_5 \\ u_6 \end{pmatrix} = \begin{pmatrix} \theta_1 \\ \theta_2 \\ \theta_3 \\ \theta_4 \\ \theta_5 \\ \theta_6 \end{pmatrix} + \frac{1}{2} \begin{pmatrix} Q^{-1}S \\ -Q^{-1}S \end{pmatrix} (I \quad -I) \begin{pmatrix} \theta_1^2 \\ \theta_2^2 \\ \theta_3^2 \\ \theta_4^2 \\ \theta_5^2 \\ \theta_6^2 \end{pmatrix} \tag{32}$$

The solution of the matrix Riccati equation (32) [14,15] gives the command pitch angles θ_i as a function of the requirement vector:

$$\begin{pmatrix} \theta_4 \\ \theta_5 \\ \theta_6 \end{pmatrix} = \left[I + Q^{-1}S \begin{pmatrix} u_1 + u_4 & 0 & 0 \\ 0 & u_2 + u_5 & 0 \\ 0 & 0 & u_3 + u_6 \end{pmatrix} \right]^{-1} \left[\begin{pmatrix} u_4 \\ u_5 \\ u_6 \end{pmatrix} + \frac{1}{2} Q^{-1}S \begin{pmatrix} (u_1 + u_4)^2 \\ (u_2 + u_5)^2 \\ (u_3 + u_6)^2 \end{pmatrix} \right] \tag{33}$$

$$\begin{pmatrix} \theta_1 \\ \theta_2 \\ \theta_3 \end{pmatrix} = \begin{pmatrix} u_1 + u_4 \\ u_2 + u_5 \\ u_3 + u_6 \end{pmatrix} - \begin{pmatrix} \theta_4 \\ \theta_5 \\ \theta_6 \end{pmatrix} \tag{34}$$

where the quantities u_i are defined in Eq. (31). Therefore, setting the command pitch angles as indicated by the solutions for θ_i will achieve the vehicle's desired force and torque vectors.

B. Propulsion via Variable-Speed/Fixed-Pitch Rotors

Variable-speed control using rigid, fixed-pitch rotors can only produce forces in the positive direction, that is, forces are restricted to the first positive octant. The force of a given rotor i is proportional to the square of rotor rotational velocity v_i in radians/second [12]:

$$f_i = k_1 v_i^2 \tag{35}$$

where k_1 is a scalar constant coefficient of proportionality that relates rotor spin speed in radians/second to force in newtons, as given in Eq. (35), and has units of $\mathrm{N}/(\mathrm{rad/s})^2$.

To solve the direct problem, the component forces, expressed as a function of rotor speed [Eq. (35)], are substituted into the force equation (17) and then are transformed into the Earth axes using Eq. (36) to give the net resultant force on the vehicle:

$$\mathbf{f}_0 = k_1 R \begin{pmatrix} 0 & 1 & 0 & 0 & 1 & 0 \\ 1 & 0 & 0 & 1 & 0 & 0 \\ 0 & 0 & 1 & 0 & 0 & 1 \end{pmatrix} \begin{pmatrix} v_1^2 \\ v_2^2 \\ v_3^2 \\ v_4^2 \\ v_5^2 \\ v_6^2 \end{pmatrix} \tag{36}$$

Although the implementation described herein uses the same k_1 for all rotors, vehicles are not limited thereto.

Referring to Fig. 6a, the propulsive reaction torque τ_i for the ith rotor is given by [12]

$$\tau_i = k_2 v_i^2 \tag{37}$$

Note that k_2, as given in Eq. (37), is a scalar constant coefficient of proportionality and relates rotor spin speed in radians/second to torque in newton meters and has units of $\mathrm{Nm}/(\mathrm{rad/s})^2$.

A similar derivation to the preceding section yields a net torque $\mathbf{t}_b$ in the vehicle in the body axes once the reaction torque components and the differential force moments are combined into one expression mapped to body axes, as given below:

$$\mathbf{t}_b = \left[\frac{k_1 l}{\sqrt{2}} \begin{pmatrix} 1 & 0 & 1 & -1 & 0 & -1 \\ 0 & -1 & 1 & 0 & 1 & -1 \\ 1 & -1 & 0 & -1 & 1 & 0 \end{pmatrix} \begin{pmatrix} v_1^2 \\ v_2^2 \\ v_3^2 \\ v_4^2 \\ v_5^2 \\ v_6^2 \end{pmatrix} + k_2 \begin{pmatrix} 0 & 1 & 0 & 0 & -1 & 0 \\ -1 & 0 & 0 & 1 & 0 & 0 \\ 0 & 0 & -1 & 0 & 0 & 1 \end{pmatrix} \begin{pmatrix} v_1^2 \\ v_2^2 \\ v_3^2 \\ v_4^2 \\ v_5^2 \\ v_6^2 \end{pmatrix} \right] \tag{38}$$

From the above analysis, the forces and torques acting on the vehicle are given together by the following composite vector:

$$\begin{pmatrix} \mathbf{f}_0 \\ \mathbf{t}_b \end{pmatrix} = \begin{pmatrix} \bar{R} & 0 \\ 0 & \bar{I} \end{pmatrix} \left[\begin{pmatrix} \bar{P} & \bar{P} \\ (\bar{Q} + \bar{S}) & -(\bar{Q} + \bar{S}) \end{pmatrix} \begin{pmatrix} v_1^2 \\ v_2^2 \\ v_3^2 \\ v_4^2 \\ v_5^2 \\ v_6^2 \end{pmatrix} \right] \tag{39}$$

where matrices $\bar{P}$, $\bar{Q}$, and $\bar{S}$ are, respectively, given by

$$\bar{P} = k_1 \begin{pmatrix} 0 & 1 & 0 \\ 1 & 0 & 0 \\ 0 & 0 & 1 \end{pmatrix} \tag{40}$$

$$\bar{Q} = \frac{k_1 l}{\sqrt{2}} \begin{pmatrix} 1 & 0 & 1 \\ 0 & -1 & 1 \\ 1 & -1 & 0 \end{pmatrix} \tag{41}$$

$$\bar{S} = k_2 \begin{pmatrix} 0 & 1 & 0 \\ -1 & 0 & 0 \\ 0 & 0 & -1 \end{pmatrix} \tag{42}$$

The rotor spin speeds are given by an inversion as follows:

$$\begin{pmatrix} v_1^2 \\ v_2^2 \\ v_3^2 \\ v_4^2 \\ v_5^2 \\ v_6^2 \end{pmatrix} = \frac{1}{2} \begin{pmatrix} I & I \\ I & -I \end{pmatrix} \begin{pmatrix} \bar{P}^{-1} \bar{R}^T & 0 \\ 0 & (\bar{Q} + \bar{S})^{-1} \end{pmatrix} \begin{pmatrix} f_{0_1} \\ f_{0_2} \\ f_{0_3} \\ t_{b_1} \\ t_{b_2} \\ t_{b_3} \end{pmatrix} \tag{43}$$

To calculate the commands for rotational speeds v_i, calculate the matrix product and then take the square-root of each component in the vector. This requires the matrices $\bar{P}^{-1}$ and $(\bar{Q} + \bar{S})^{-1}$ to exist. Note that the inverse of P always exists, and the condition for the existence of $(\bar{Q} + \bar{S})^{-1}$ is

$$\det(\bar{Q} + \bar{S}) = \frac{(k_1 l)^3}{\sqrt{2}} + k_2 \left(\frac{3(k_1 l)^2}{2} - k_2^2 \right) \neq 0$$

which is easily fulfilled if

$$k_2 < \sqrt{\tfrac{3}{2}} k_1 l$$

which is indeed the case as, in practice, k_2 is negligible compared with $k_1 l$.

IV. Dynamics Model

The dynamic model of an orthogonal face-centered hexrotor vehicle is obtained in the present section for the two cases of variable-pitch/constant-speed rotors and fixed-pitch/variable-speed rotors. For simplicity of exposition of the ideas, second-order effects such as air drag on the vehicle fuselage and rotor mutual interference are not considered; therefore, simplifying the model to only inertial and dynamical effects. Likewise, the rotors will be modeled as simple steady-state force and torque sources. Analysis at the end of this section also shows that the magnitude of changes in rotor angular momentum is small compared with the magnitude of the control torques produced; hence, this effect can be neglected from the control synthesis in the interest of simplified models.

A. Variable-Pitch Rotors

Let $\mathbf{r}_0$ be the current position of a vehicle in Earth axes, and let $\boldsymbol{\omega}_b$ be the current angular velocity of the vehicle read in the vehicle body axes such that

$$\mathbf{r}_0 = \begin{pmatrix} x_0 \\ y_0 \\ z_0 \end{pmatrix} \tag{44}$$

$$\boldsymbol{\omega}_b = \begin{pmatrix} \omega_{b,x} \\ \omega_{b,y} \\ \omega_{b,z} \end{pmatrix} \tag{45}$$

Also define the skew-symmetric matrix

$$s(\boldsymbol{\omega}_b) = \begin{pmatrix} 0 & -\omega_{b,z} & \omega_{b,y} \\ \omega_{b,z} & 0 & -\omega_{b,x} \\ -\omega_{b,y} & \omega_{b,x} & 0 \end{pmatrix} \tag{46}$$

assuming negligible aerodynamic drag on the vehicle fuselage. This assumption is acceptable for the current simplified analysis, because drag forces tend to slow down performance but do not have any destabilizing effect. Evaluating the angular momentum, the attitude dynamics are given by the following Newton–Euler equations [16,17]:

$$\mathbf{t}_0 = \frac{\mathrm{d}}{\mathrm{d}t}(J_0 \boldsymbol{\omega}_0) \tag{47}$$

$$\Leftrightarrow \mathbf{t}_b = J_b \dot{\boldsymbol{\omega}}_b + s(\boldsymbol{\omega}_b) J_b \boldsymbol{\omega}_b \tag{48}$$

B. Variable-Speed Rotors

For this analysis, let $\mathbf{r}_0$ be the current position of a vehicle in the Earth axes and let $\boldsymbol{\omega}_b$ be the current angular velocity such as in Eqs. (44) and (45). The angular momentum of the rotors is now taken into account given that the variable speed of the rotors prevents

perfect cancellation of gyroscopic effects. Evaluating the angular momentum assuming negligible aerodynamic drag, the attitude dynamics are given by the following Newton–Euler equation [16,17]:

$$\mathbf{t}_0 = \frac{\mathrm{d}}{\mathrm{d}t}\left(J_0\boldsymbol{\omega}_0 + RJ_r \begin{bmatrix} v_5 - v_2 \\ v_1 - v_4 \\ v_3 - v_6 \end{bmatrix} \right) \tag{49}$$

where J_r is the scalar moment of inertia of a single rotor about its shaft axis, R is the rotational matrix mapping vectors read in body axes to the same vector read in Earth axes, $J_0\boldsymbol{\omega}0$ is the angular momentum in Earth axes, and $v_1, v_2, \ldots, v_6$ are the rotor speed commands as calculated in Eq. (43). Equation (49) can be transformed equivalently to

$$\mathbf{t}_b = \left\{ J_b\dot{\boldsymbol{\omega}}_b + J_r \begin{bmatrix} \dot{v}_5 - \dot{v}_2 \\ \dot{v}_1 - \dot{v}_4 \\ \dot{v}_3 - \dot{v}_6 \end{bmatrix} \right\} + s(\boldsymbol{\omega}_b) \left\{ J_b\boldsymbol{\omega}_b + J_r \begin{bmatrix} v_5 - v_2 \\ v_1 - v_4 \\ v_3 - v_6 \end{bmatrix} \right\} \tag{50}$$

Since, in practice, J_b will typically be several orders of magnitude larger than J_r, the gyroscopic effects will have negligible effects on the dynamics and hence can be ignored. Small differential variation in the angular velocity or angular acceleration of corresponding rotor pairs will be overridden by a corresponding small variation in the vehicle angular velocity or vehicle angular acceleration in the same direction.

Additionally, even when this assumption is not fulfilled, gyroscopic effects tend to have a stabilizing effect on attitude, due to conservation of angular momentum rather than a detrimental effect [16,17]. Henceforth, it will be assumed that the dynamical model of the attitude is reduced to

$$\mathbf{t}_b = J_b\dot{\boldsymbol{\omega}}_b + s(\boldsymbol{\omega}_b)J_b\boldsymbol{\omega}_b \tag{51}$$

The reduced model in Eq. (51) is the same as that deduced for the variable-pitch rotor in Eq. (48), given that the gyroscopic effects present in the variable-speed rotors are neglected around near-hover conditions. Therefore, in accordance with these models, there is no need to synthesize two different controllers.

C. Translational Dynamics

The translational model describes the hexrotor vehicle as a particle with mass moving in free 3-D space. For simplicity of exposition of ideas, air drag on the fuselage is not considered, therefore limiting the model only to inertial and dynamic effects. Likewise, the rotors will be modeled as simple steady-state force sources [16,17]. Newton's second law of motion gives

$$\mathbf{f}_0 + \begin{pmatrix} 0 \\ 0 \\ mg \end{pmatrix} = m\ddot{\mathbf{r}}_0 \tag{52}$$

where m is the mass of the vehicle, $\mathbf{r}_0$ is the position in Earth axes, and g is the gravitational acceleration.

V. Control Strategy

The controller of the hexrotor vehicle will take advantage of the analytically decoupled force and torque subsystems achieved by the use of six rotors, as demonstrated in Eq. (26) for variable-pitch rotors and in Eq. (39) for variable-speed rotors. The direct consequence of actuation independency is that the model can be decomposed into the rotational dynamics described by Eq. (48) and completely decoupled from the translational dynamics described by Eq. (52) [16].

A. Position Control

The control scheme illustrated in Fig. 8 uses full state feedback linearization to compensate for the gravitational force and a state feedback controller to follow the designed trajectory. Perfect cancellation of the gravity vector is assumed to be achieved. Take the translational dynamics model (52) and assume that the input force vector $\mathbf{f}_0 = [f_{0_1} \quad f_{0_2} \quad f_{0_3}]$ is composed of gravitational-force cancellation plus a trajectory-tracking state feedback control law [16,18]:

$$\begin{pmatrix} f_{0_1} \\ f_{0_2} \\ f_{0_3} \end{pmatrix} = -\begin{pmatrix} 0 \\ 0 \\ mg \end{pmatrix} + m[\ddot{\mathbf{r}}_0^d - 2\xi c(\dot{\mathbf{r}}_0 - \dot{\mathbf{r}}_0^d) - c^2(\mathbf{r}_0 - \mathbf{r}_0^d)] \tag{53}$$

Applying the force equation (53) into the translational dynamics equation (52) results in the following linear closed loop for position dynamics:

$$(\ddot{\mathbf{r}}_0 - \ddot{\mathbf{r}}_0^d) + 2\xi c(\dot{\mathbf{r}}_0 - \dot{\mathbf{r}}_0^d) + c^2(\mathbf{r}_0 - \mathbf{r}_0^d) = 0 \tag{54}$$

where $\ddot{\mathbf{r}}_0^d$ is a desired acceleration, $\dot{\mathbf{r}}_0^d$ is a desired velocity, $\mathbf{r}_0^d$ is a desired position for the designated trajectory, and the chosen controller gains ξ and c are equivalent to the damping factor and natural frequency, respectively, of the closed-loop dynamics. To run experiments with acceptable closed-loop pole placement, the controller gains are chosen as $\xi = 0.7$ and $c = 2\pi(0.2)$. In this way the position control is globally stable, because all the poles are in the left-hand plane of the complex plane, and the time constant of the closed-loop dynamics is 5 s [16,18].

Integral control can be used for exact cancellation of the gravity vector $[0 \quad 0 \quad mg]^T$, but is not considered for simplicity of exposition. Although the above control law is designed using simple classical ideas, more robust and optimal control methods could be designed on the open-loop plant to yield robustness and perhaps energy-optimal guaranties (see, for example, [15,19–21]). Second-order systems as the resulting closed-loop dynamics above are negative imaginary systems [22], which can be exploited in inner/outer-loop control methods in which the inner loop is fast approximate control and the outer loop is slower, but it ensures that the correct steady-state equilibria are reached. Offline validation methods for internal stability using closed-loop data from experiments using a previous stabilizing controller are described in [23,24], and these methods can be helpful when tuning controllers in practice to avoid the risk that excessive model mismatch may result in instability.

B. Attitude Control

The desired attitude trajectory is expressed by the attitude quaternion $\mathbf{q}^d$ (we use the quaternion structure of the scalar element as the top element and the vector below it), angular speed $\boldsymbol{\omega}_b^d$ and angular acceleration $\dot{\boldsymbol{\omega}}_b^d$. The procedure to obtain this trajectory will be explained in detail in the next section. The attitude control is performed in the body axes, because both the measurements and actuators are read and controlled in body axes [16].

The objective of the control law is to follow the designated attitude trajectory. The control problem is divided into two loops shown in Fig. 9, because the dynamics of the angular rate are faster than the attitude dynamics. Full state feedback linearization closes an inner secondary loop for angular speed, then state feedback in quaternion space closes the outer loop of attitude control [16]. If chosen appropriately, from the point of view of the attitude controller, the model of the vehicle's speed is reduced to first-order linear dynamics, followed by the model of attitude kinematics. To control the angular rate, assume the synthesized torque vector $\mathbf{t}_b = [t_{b_1} \quad t_{b_2} \quad t_{b_3}]^T$

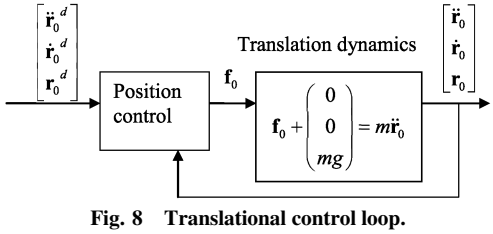

Fig. 8 Translational control loop.

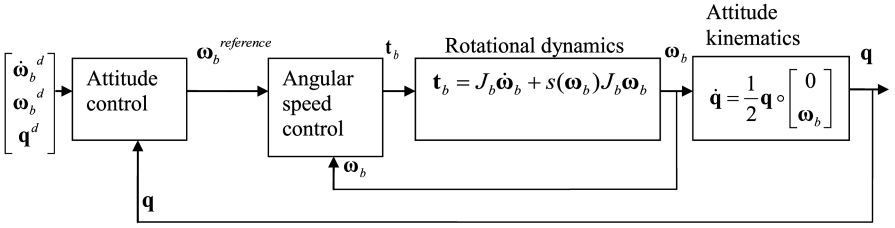

Fig. 9 Attitude control loops.

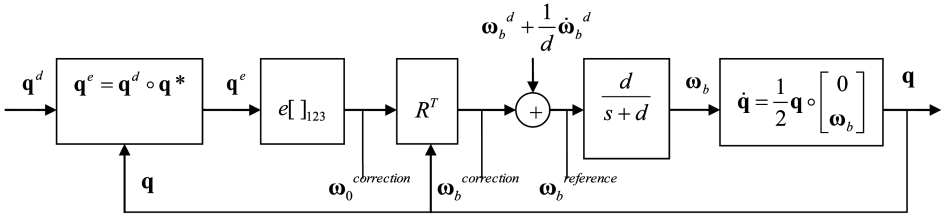

Fig. 10 Attitude control.

compensates for the nonlinear effect of the Coriolis term and at the same time minimizes the speed error, using a state feedback controller [17,18]. Choosing

$$\begin{pmatrix} t_{b_1} \\ t_{b_2} \\ t_{b_3} \end{pmatrix} = s(\boldsymbol{\omega}_b)J_b\boldsymbol{\omega}_b + dJ_b(\boldsymbol{\omega}_b^{\text{reference}} - \boldsymbol{\omega}_b) \tag{55}$$

where the parameter d represents a gain matrix for the state feedback controller, and the closed-loop system is obtained by substituting the torque $\mathbf{t}_b$ from Eq. (55) into angular dynamics equation (48) to give the following linear closed-loop dynamics:

$$\dot{\omega}_b + d\omega_b = d\omega_b^{\text{reference}} \tag{56}$$

Equation (56) represents a first-order system, where the gain d is equivalent to the closed-loop time constant of the angular rate. For this particular implementation, it has been chosen as $d = 2\pi(0.2)$, and so a closed-loop response will have a time constant of 5 s.

The outer loop, controlling the attitude, defines a normalized quaternion error $\mathbf{q}^e$ to be given by

$$\mathbf{q}^e = \mathbf{q}^d \circ \mathbf{q}^* \tag{57}$$

where $\mathbf{q}^d$ represents a desired vehicle attitude, $\mathbf{q}^*$ is the quaternion conjugate of the current vehicle attitude, and $\circ$ denotes quaternion multiplication.

The desired angular attitude $\mathbf{q}^d$, expressed as a quaternion, is one input to the attitude control system. The normalized quaternion error attitude is calculated by Eq. (57). Letting $[\cdot]_{123}$ denote the bottom three elements of a normalized quaternion, this part extracts the axis of rotation. Consequently, setting $\boldsymbol{\omega}_0^{\text{correction}} = e[\mathbf{q}]_{123}$ means that we choose an angular speed correction that is proportional (with constant of proportionality e) and aligned in the direction with the axis of rotation of the normalized quaternion error $\mathbf{q}^e$. Since the angular speed correction $\boldsymbol{\omega}_0^{\text{correction}}$ is expressed in Earth axes, it is required to be transformed into body coordinates by rotational matrix R^T to obtain the desired angular velocity $\boldsymbol{\omega}_b^{\text{correction}}$, expressed in body axes. Then $\boldsymbol{\omega}_b^{\text{correction}}$ is added to the required trajectory (defined by the desired angular rate and desired angular acceleration), to produce a reference angular rate $\boldsymbol{\omega}_b^{\text{reference}}$ in the following equation, used as input by the speed controller (55) in the dynamic relations of Eq. (56):

$$\omega_b^{\text{reference}} = \omega_b^{\text{correction}} + \omega_b^d + \frac{1}{d}\dot{\omega}_b^d \tag{58}$$

Analyzing Fig. 10, a simplification can be found. Define a mismatch normalized quaternion $\mathbf{q}^m$ by

$$\mathbf{q}^m = \mathbf{q}^* \circ \mathbf{q}^d \tag{59}$$

Since quaternion algebra gives [25]

$$\mathbf{q} \circ \begin{pmatrix} \delta \\ \mathbf{n} \end{pmatrix} \circ \mathbf{q}^* = \begin{pmatrix} \delta \\ R\mathbf{n} \end{pmatrix} \tag{60}$$

for any arbitrary real scalar δ and any arbitrary vector $\mathbf{n}$, it follows that

$$\mathbf{q}^m = \mathbf{q}^* \circ \mathbf{q}^d = \mathbf{q}^* \circ \mathbf{q}^d \circ \mathbf{q}^* \circ \mathbf{q} \tag{61}$$

$$\mathbf{q}^m = \mathbf{q}^* \circ \mathbf{q}^e \circ \mathbf{q} \tag{62}$$

Therefore, $[\mathbf{q}^m]_{123} = R^T[\mathbf{q}^e]_{123}$.

Hence, it is possible to calculate the mismatch normalized quaternion $\mathbf{q}^m$ instead of executing the normalized quaternion error $\mathbf{q}^e$ and rotate its bottom three elements by rotational matrix R^T. Figure 10 can now be simplified, as indicated in Fig. 11.

Robustness issues can appear from the insertion of the inexact compensation for Coriolis force and uncertainty in the rotors. The inexact cancellation of forces produces a small amount of coupling between force and torque, which, in principle, was assumed to be cancelled by the torque controller. This effect can affect the overall performance of the hexrotor, as illustrated by a simulated rotational maneuver in Sec. VIII. To address this problem, robust controllers [21] use knowledge of disturbances, including motor time constants and Coriolis structure, to synthesize a controller d that will stabilize

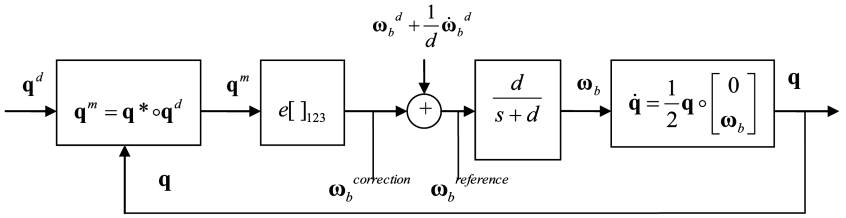

Fig. 11 Attitude control simplified.

the plant and keep acceptable performance, even with small torque and force coupling.

VI. Stability Analysis of Attitude Control

A stability analysis for attitude and angular velocity control is performed in the feedback control proposed. Let the Lyapunov candidate function V [16] be defined as

$$V = \frac{(\boldsymbol{\omega}_b - \boldsymbol{\omega}_b^d)^T(\boldsymbol{\omega}_b - \boldsymbol{\omega}_b^d)}{2d} + e([\mathbf{q}^m]_1^2 + [\mathbf{q}^m]_2^2 + [\mathbf{q}^m]_3^2 + ([\mathbf{q}^m]_0 - 1)^2) \tag{63}$$

where $[\mathbf{q}]_i$ denotes the ith element of the quaternion $\mathbf{q}$, 0 denotes the first element, and 3 denotes the last one.

Note that $V \geq 0 \,\forall\, \boldsymbol{\omega}_b$, $\mathbf{q}^m$, and $V = 0$ if and only if the trajectory goal $\boldsymbol{\omega}_b = \boldsymbol{\omega}_b^d$ and $\mathbf{q} = \mathbf{q}^d$ (since $\mathbf{q}^m = [1 \quad 0 \quad 0 \quad 0]^T$) is achieved. Since $\mathbf{q}^m$ is a normalized quaternion, we have $\|\mathbf{q}^m\| = 1$, and hence V can be rearranged as

$$V = \frac{(\boldsymbol{\omega}_b - \boldsymbol{\omega}_b^d)^T(\boldsymbol{\omega}_b - \boldsymbol{\omega}_b^d)}{2d} + 2e(1 - [\mathbf{q}^m]_0) \tag{64}$$

If the Lyapunov candidate function is now differentiated, the resulting function is

$$\dot{V} = (\boldsymbol{\omega}_b - \boldsymbol{\omega}_b^d)^T\left(\frac{\dot{\boldsymbol{\omega}}_b}{d} - \frac{\dot{\boldsymbol{\omega}}_b^d}{d}\right) - 2e[\dot{\mathbf{q}}^m]_0 \tag{65}$$

Substituting $\dot{\boldsymbol{\omega}}_b$ from the linear dynamics equation (56) we obtain

$$\dot{V} = (\boldsymbol{\omega}_b - \boldsymbol{\omega}_b^d)^T\left(-\boldsymbol{\omega}_b + \boldsymbol{\omega}_b^{\text{reference}} - \frac{\dot{\boldsymbol{\omega}}_b^d}{d}\right) - 2e[\dot{\mathbf{q}}^m]_0 \tag{66}$$

Further substituting the reference angular speed $\boldsymbol{\omega}_b^{\text{reference}}$ using Fig. 11 and Eq. (58),

$$\dot{V} = (\boldsymbol{\omega}_b - \boldsymbol{\omega}_b^d)^T(-\boldsymbol{\omega}_b + e[\mathbf{q}^m]_{123} + \boldsymbol{\omega}_b^d) - 2e[\dot{\mathbf{q}}^m]_0 \tag{67}$$

and regrouping similar terms,

$$\dot{V} = -(\boldsymbol{\omega}_b - \boldsymbol{\omega}_b^d)^T(\boldsymbol{\omega}_b - \boldsymbol{\omega}_b^d) + e(\boldsymbol{\omega}_b - \boldsymbol{\omega}_b^d)^T[\mathbf{q}^m]_{123} - 2e[\dot{\mathbf{q}}^m]_0 \tag{68}$$

Therefore, the derivative of the Lyapunov function is negative, $\dot{V} < 0 \,\forall\, \boldsymbol{\omega}_b \neq \boldsymbol{\omega}_b^d$, since

$$(\boldsymbol{\omega}_b - \boldsymbol{\omega}_b^d)^T[\mathbf{q}^m]_{123} - 2[\dot{\mathbf{q}}^m]_0 = 0$$

because $\mathbf{q}^m = \mathbf{q}^* \circ \mathbf{q}^d$ and $[\mathbf{q}^m]_0 = \mathbf{q}^T\mathbf{q}^d$, which implies that

$$\begin{aligned}[\dot{\mathbf{q}}^m]_0 &= \mathbf{q}^T\dot{\mathbf{q}}^d + (\mathbf{q}^d)^T\dot{\mathbf{q}} = [\mathbf{q}^* \circ \dot{\mathbf{q}}^d]_0 + [(\mathbf{q}^d)^* \circ \dot{\mathbf{q}}]_0 \\ &= \frac{1}{2}\left[\mathbf{q}^* \circ \mathbf{q}^d \circ \begin{bmatrix} 0 \\ \boldsymbol{\omega}_b^d \end{bmatrix}\right]_0 + \frac{1}{2}\left[\mathbf{q}^{d*} \circ \mathbf{q} \circ \begin{bmatrix} 0 \\ \boldsymbol{\omega}_b \end{bmatrix}\right]_0 \\ &= \frac{1}{2}\left[\mathbf{q}^m \circ \begin{bmatrix} 0 \\ \boldsymbol{\omega}_b^d \end{bmatrix}\right]_0 + \frac{1}{2}\left[\mathbf{q}^{m*} \circ \begin{bmatrix} 0 \\ \boldsymbol{\omega}_b \end{bmatrix}\right]_0 \\ &= -\frac{1}{2}(\boldsymbol{\omega}_b^d)^T[\mathbf{q}^m]_{123} + \frac{1}{2}\boldsymbol{\omega}_b^T[\mathbf{q}^m]_{123}\end{aligned} \tag{69}$$

$$[\dot{\mathbf{q}}^m]_0 = \tfrac{1}{2}(\boldsymbol{\omega}_b - \boldsymbol{\omega}_b^d)^T[\mathbf{q}^m]_{123} \tag{70}$$

The function $V(t)$ reaches an equipotential whenever $\boldsymbol{\omega}_b(t) = \boldsymbol{\omega}_b^d(t)$, since $\dot{V}(t) = 0$. Now it will be shown that

$$\boldsymbol{\omega}_b(t) = \boldsymbol{\omega}_b^d(t) \,\forall\, t \Rightarrow \mathbf{q}(t) = \mathbf{q}^d(t) \,\forall\, t$$

If the measured angular speed is equal to the desired angular speed $\boldsymbol{\omega}_b(t) = \boldsymbol{\omega}_b^d(t) \,\forall\, t$, then $\dot{\boldsymbol{\omega}}_b(t) = \dot{\boldsymbol{\omega}}_b^d(t) \,\forall\, t$, and hence $\boldsymbol{\omega}_b^{\text{correction}}(t) = 0$ via Eq. (56) and the fact that

$$\boldsymbol{\omega}_b^{\text{reference}} = \boldsymbol{\omega}_b^{\text{correction}} + \boldsymbol{\omega}_b^d + \frac{1}{\mathrm{d}}\dot{\boldsymbol{\omega}}_b^d$$

Then $\boldsymbol{\omega}_b^{\text{correction}} = e[\mathbf{q}^m]_{123} = 0$ yields $\mathbf{q}^m(t) = [1 \quad 0 \quad 0 \quad 0]^T$ for the normalized quaternion $\mathbf{q}^m$. The only way to achieve this condition is to make the measured trajectory $\mathbf{q}$ equal to the desired quaternion trajectory $\mathbf{q}^d$, i.e., $\mathbf{q}(t) = \mathbf{q}^d(t)$. Hence, we have shown that stabilizing angular velocity control also implies stabilizing attitude control.

VII. Relations Between Quaternion Rates and Angular Velocities

The specific mission is defined by the required trajectory in quaternions. To calculate the required speed and acceleration for the trajectory, the quaternion defining the path has to be differentiated using [25]

$$\dot{\mathbf{q}}^d = \frac{1}{2}\mathbf{q}^d \circ \begin{bmatrix} 0 \\ \boldsymbol{\omega}_b^d \end{bmatrix} \tag{71}$$

Making the angular speed subject and then differentiating another time to find the angular velocity, we get angular position $\mathbf{q}^d$, angular velocity $\boldsymbol{\omega}_b^d = 2[\mathbf{q}^{d*} \circ \dot{\mathbf{q}}^d]_{123}$, angular acceleration $\dot{\boldsymbol{\omega}}_b^d = 2[\mathbf{q}^{d*} \circ \ddot{\mathbf{q}}^d]_{123}$, and for an attitude trajectory designed in quaternion space, $(\mathbf{q}^d, \dot{\mathbf{q}}^d, \ddot{\mathbf{q}}^d)$.

VIII. Results and Discussion

We report the simulations of translational and rotational maneuvers. The numeric values of mechanical parameters used in the translational model (52) and in the rotational model (48) are take-off mass $m = 5.006$ kg, gravitational acceleration $g = 9.81$ m/s^2, motor time constant 0.1 s, and moment of inertia in the vehicle reference plane of

$$J_b = \begin{bmatrix} 0.2 & 0.05 & 0.05 \\ 0.05 & 0.2 & 0.05 \\ 0.05 & 0.05 & 0.2 \end{bmatrix} \text{ kg m}^2$$

The rotor geometrical position X_r is

$$0.3\begin{bmatrix} 1 & 0 & -1 & -1 & 0 & 1 \\ 0 & 1 & 1 & 0 & -1 & -1 \\ -1 & -1 & 0 & 1 & 1 & 0 \end{bmatrix} \text{m}$$

and the rotor direction N_r is

$$\begin{bmatrix} 0 & 1 & 0 & 0 & 1 & 0 \\ 1 & 0 & 0 & 1 & 0 & 0 \\ 0 & 0 & 1 & 0 & 0 & 1 \end{bmatrix}$$

Aerodynamic constants for the fixed-pitch/variable-speed rotors are given in Table 1. Aerodynamic constants for the fixed-speed/variable-pitch rotors are given in Table 2.

To control the hexrotor vehicle, the control parameters are described in Table 3. The parameters are chosen so that perfect cancellation of gravity force mg and Coriolis force $s(\boldsymbol{\omega}_b)J_b\boldsymbol{\omega}_b$ are achieved. However, in the prototype, perfect cancellation will be not possible, but only a good approximation, and therefore small deviations on signals can happen. The controller for translation is described in Eq. (53), the controller for angular rate is described in Eq. (55), and the controller for quaternion attitude is described by the diagonal gain matrix e in Fig. 11.

A. Steady State

An experiment was conducted to evaluate the extent of aerodynamic interference between the six rotors when operating in near-hover conditions, i.e., to evaluate the validity of the assumption used in the modeling that all rotors act independently (at least in level hover). Figure 12 shows a flight-capable airframe rigidly mounted to a six-component balance on a test rig. The speed of each rotor can be

Table 1 Aerodynamic constants of fixed pitch and variable speed

Parameter	Value
Thrust constant k_1	5×10^{-3} N/(rad/s)^2
Torque constant k_2	1×10^{-2} Nm/(rad/s)^2

Table 2 Aerodynamic constants of fixed speed and variable pitch

Parameter	Value
Thrust constant $\hat{k}$	6.40×10^{-5} N/rad
Torque constant k_T	1.74×10^{-6} Nm/rad^2

Table 3 Control parameters

Parameter	Value
Translational damping ξ	0.7
Translational natural frequency c	$2\pi(0.2)$ rad/s
Angular speed damping d	$2\pi(0.2)$
Quaternion proportionality constant e	2π

controlled independently, and the speed, current, and voltage of all six propulsion units are recorded, as well as six components of force and torque from the balance, Torque and force are demanded through relations (6–9), and the generated torque and force are then measured from the balance. The measured torques and forces are then compared with those obtained from substituting experimental rotor speed into Eqs. (6–9).

Results presented in the format $\mathbf{t}_0 = [t_{0_1}\ t_{0_2}\ t_{0_3}]^T$ shows the results for a pure yawing moment (t_{0_3}) and pure pitching moment demand (t_{0_2}) are shown in Fig. 13. The yawing demand is varied from -11 to 11 Nm, and the rest of the moments have a zero demand. The result is a change in moment only around the Z axis, and the rest of the moments are kept null. The rotors that are not contributing to the yawing moment are still running, keeping the rest of the moments equal to zero. The experiment demonstrates that the torque generated by the array of rotors follows the relations described by Eqs. (6), (7), and (9), where the key assumption is that the torque vector $\mathbf{t}$ depends only on the thrust F_i and drag torque τ_i. The same experiment is repeated for a pitching moment demand in Fig. 13, with similar results. These results show that for the relatively benign case of level hover, use of a simple uncoupled rotor aerodynamic model for control is fit for purpose. At more extreme flight conditions rotor interaction are likely to be larger and nonlinear; hence, the simple modeling approach adopted in this paper may not be sufficient.

Fig. 12 Experimental setup for thrust and torque measurements.

Figure 14 shows the experiment when thrust is demanded in the Z axis. The force vector is expressed in the form $\mathbf{f}_0 = [f_{0_1}\ f_{0_2}\ f_{0_3}]^T$. The experiment follows the force relation proposed by Eqs. (6–8). The thrust in the Z axis is varied from -10 to -100 N. The result is a thrust generated only in the Z axis, and resultant thrusts in the X and Y axes are kept null by the rotors.

The above experimental results provide evidence to support the validity of using the simplified aerodynamic rotor model proposed in Sec. II for flight conditions around hover with the vehicle reference plane horizontal.

B. Simulated Translational Maneuver

The degree of coupling between the proposed position control and attitude regulation is evaluated through a simulated translational maneuver corresponding to a position demand of 1 m in X, -1.7 m in Y, and 0 m in Z (Fig. 15). The rotor speeds during the maneuver are shown in Fig. 16.

The results for X and Z show a step response with damping ratio $\xi = 0.69$ and natural frequency of 1.4 s^{-1}, which are values very close to those expected by the control definition in Table 3, and the attitude is held constant, as required.

C. Simulated Rotational Maneuver

The simulated maneuver for evaluation of the attitude control corresponds to a rotational sequence of $[\,\pi/8 \quad 0 \quad \pi/4\,]$ radians about the x, y, and z body axes, respectively, with the position of the vehicle held constant. The initial attitude of the vehicle is with the vehicle reference plane horizontal. The intention of this experiment is to show the independence of attitude control from thrust control, even in large rotations.

Simulation results for position and attitude are shown in Fig. 17, with corresponding rotor speeds shown in Fig. 18. A noticeable feature of the simulation results is weak coupling between the attitude response and the position of the vehicle. This characteristic appears because the rotors generating the lift forces have time constants not cancelled fast enough by the angular-rate control, due the fact that the time constant of the attitude closed loop is very close to that of the rotors. However, at the end of the simulated maneuver the steady-state position reaches the reference signal at 0 m, showing that controllers are robust enough to cancel effect of small deviations from the ideal model. With reference to the rotor speeds shown in Fig. 18, it can be seen that at the start of the maneuver all rotor speeds are equal, consistent with the symmetry associated with generation of a net force vector normal to the vehicle reference plane. At the end of the maneuver the required net force vector is nonnormal to the vehicle reference plane, and hence the required rotor speeds are unequal.

Analysis of the attitude step response gives a closed-loop damping ratio of 0.25 and natural frequency of 1.85 s^{-1}, with zero steady-state error. This second-order response is explained by the fact that the attitude controller is naturally adding an extra order to the first-order inner angular-rate loop, because the attitude itself is the integral of the angular speed. If the attitude controlled is required to reduce its overshoot, the proportional constant e has to be decreased; e can be seen as the open-loop gain for the attitude control system.

D. Free to Pitch, Roll, or Yaw Experiments

To evaluate the attitude control dynamics before flight test, the prototype flight vehicle was mounted on a mechanical gimbal, giving approximately ± 30 degrees of freedom in roll and pitch and around

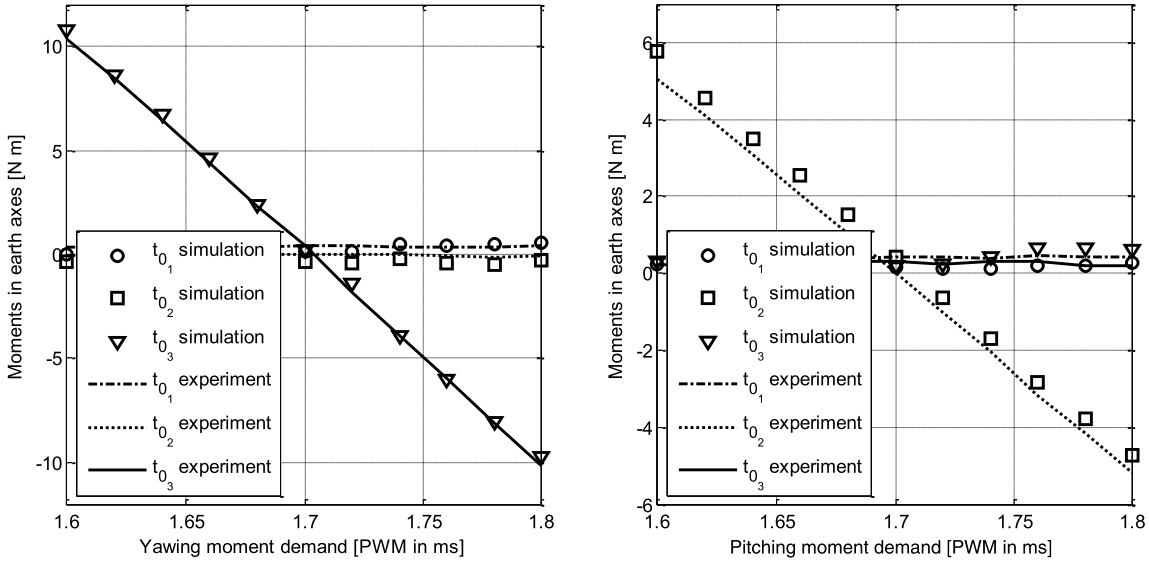

Fig. 13 Moment independence.

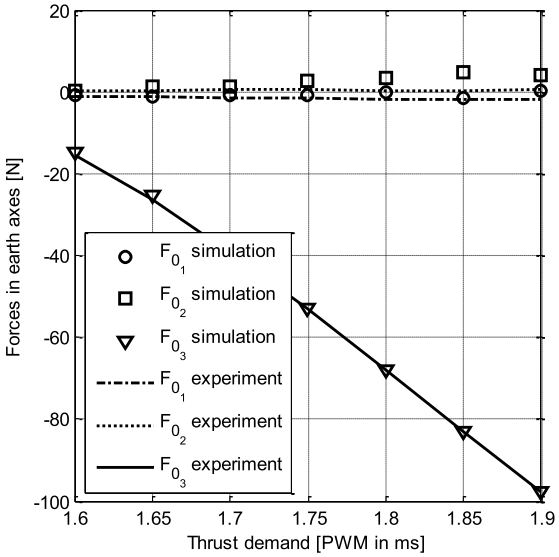

Fig. 14 Thrust independence.

±15 deg in yaw. The primary purpose of these tests was to verify the implementation of the attitude control laws onboard the vehicle flight control computer, to validate choice of rate control gains and to provide a very basic flight-training simulator for the remote pilot.

E. Flight-Test Report

The airframe shown on the test stand in Fig. 12 was flown as a free-flight vehicle in November 2009. The main objectives of the flight test was to demonstrate that a viable vehicle could be developed using commercially available actuator and sensor components and that the simplified rotor aerodynamic modeling used in this paper is fit for the purposes of controller design around hover. The all up weight of the flight-test vehicle was 5.5 kg with a weight breakdown of 55% propulsion group (including speed controllers), 9% structures, 26% battery, and a payload fraction of around 10% used for instrumentation. The flight duration in hover was approximately 5 min. Tests were conducted indoors, without access to absolute measurement of position and attitude, but with onboard measurement of three-axis acceleration and angular rates. Pilot input was provided through demand of angular rates and overall thrust magnitude in the same manner in which a conventional planar helicopter is flow. As an indication of the inherent robustness of the actuation strategy, the

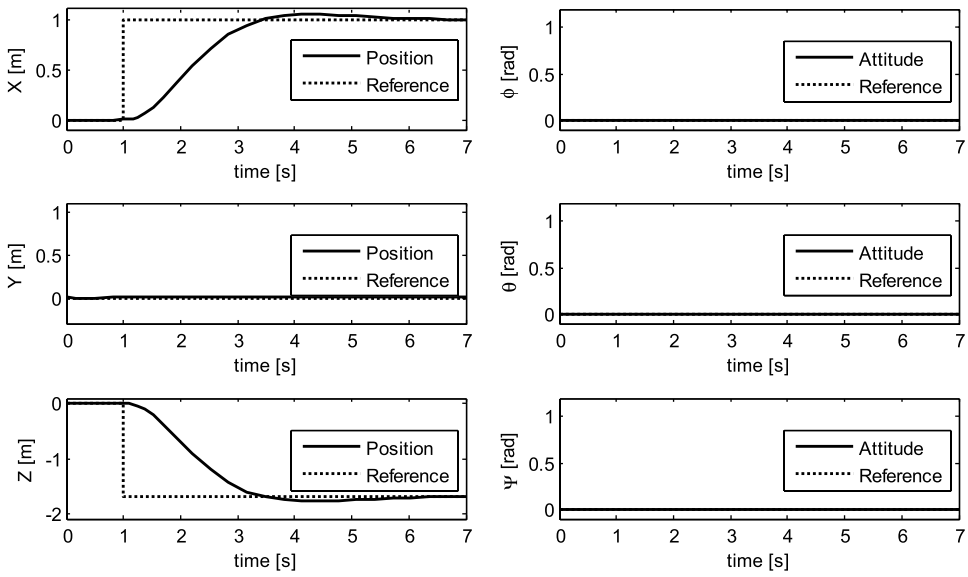

Fig. 15 Simulated translational maneuver.

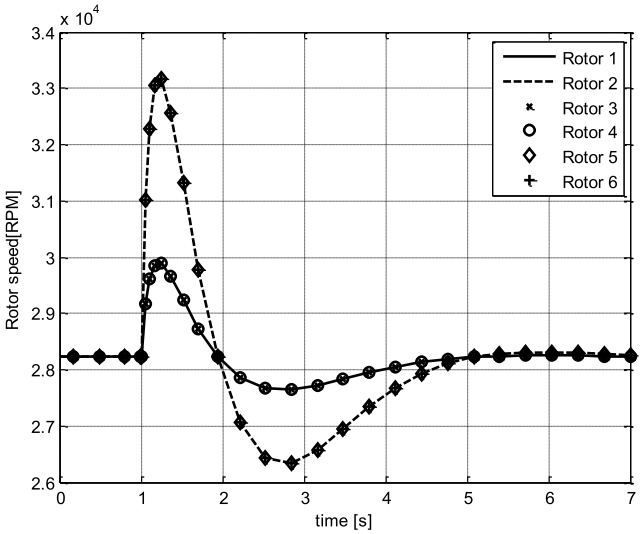

Fig. 16 Rotor speed for translational maneuver.

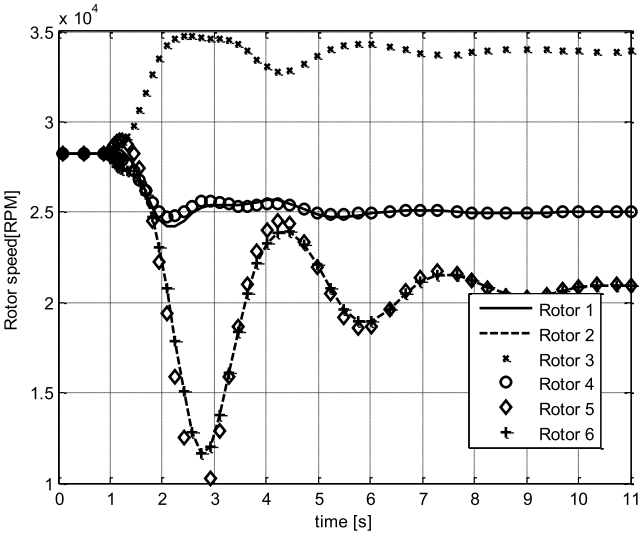

Fig. 18 Rotor speed in attitude maneuver.

vehicle was initially flown for short test flights using simple open-loop control of rates and thrust magnitude. Progressive introduction of closed-loop control of rates and thrust magnitude improved the vehicle handling qualities until steady-hover and slow-translation flight could be achieved.

IX. Conclusions

This paper has introduced a new hexrotor class of rotary-wing vehicles that provides the capability for independent control of both position and attitude for hover and slow forward flight. It has been shown that there are a number of different configurations of hexrotor vehicle possible, depending on the relative orientation of the reference planes on which the rotors are arranged and the arrangement of rotors on these planes (face-centered or edge-centered layout). A relationship between reference-plane orientation and orthogonality of force and torque control has been defined, and it is shown how a designer may tailor a design according to competing requirements for maneuverability and propulsive efficiency.

A key theoretical contribution of the paper is the analytical derivation of the static mappings between demanded control forces and torques and the required rotor thrusts. The existence of a solution to this inverse problem is not a given from inspection of the vehicle geometry, and the general proof given here is valid for arbitrary vehicle geometry and both variable-pitch/fixed-speed and fixed-pitch/variable-speed rotors. Position and attitude controllers have been successfully synthesized for the vehicle based on full state feedback control, with controller dynamic performance validated in simulation. Control performance is robust to the unmodeled dynamics associated with varying rotor angular momentum for a fixed-pitch/variable-speed control implementation.

The hexrotor vehicle concept has been prototyped in a face-centered planar configuration with fixed-pitch/variable-speed rotors. Ground tests on this vehicle have demonstrated the ability of the configuration to generate independent force and torque control under hover conditions using practical rotor systems. Furthermore, this vehicle has been successfully flown in hover with manual control of position and attitude and with inner closed-loop control of angular rates.

Acknowledgments

The second and third authors gratefully acknowledge the financial support of the Engineering and Physical Sciences Research Council and The Royal Society.

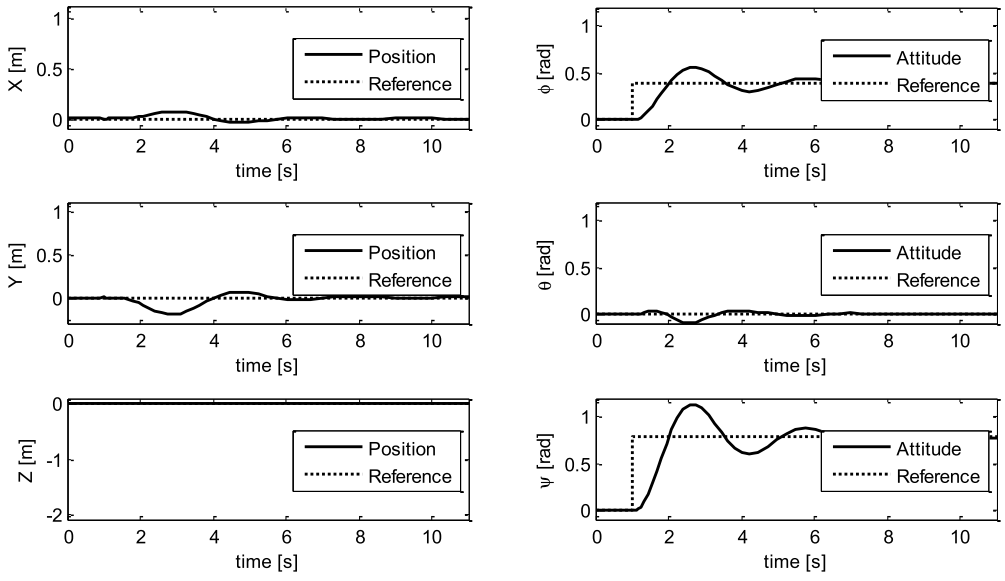

Fig. 17 Simulated response to a step change in attitude.

References

[1] Crowther, W., Lanzon, A., Pilmoor, M., and Geoghegan, P., "Rotary Wing Vehicle," U.K. Patent GB2462452A, 10 Feb. 2010.

[2] Beyer, E., and Costello, M., "Measured and Simulated Motion of a Hopping Rotochute," *Journal of Guidance, Control, and Dynamics*, Vol. 32, No. 5, 2009, pp. 1560–1569. doi:10.2514/1.41331

[3] Hoffmann, G. M., Huang, H., Waslander, S. L., and Tomlin, C. J., "Quadrotor Helicopter Flight Dynamics and Control: Theory and Experiment," AIAA Guidance, Navigation, and Control Conference and Exhibit, Hilton Head, SC, AIAA Paper 2007-6461, 2007.

[4] Waslander, S., Hoffmann, G., Jang, J. S., and Tomlin, C. J., "Multi-Agent Quadrotor Testbed Control Design: Integral Sliding Mode vs. Reinforcement Learning," *IEEE/RSJ International Conference on Intelligent Robots and Systems*, IEEE, Piscataway, NJ, 2005, pp. 3712–3717. doi:10.1109/IROS.2005.1545025

[5] Valavanis, K. P., *Advances in Unmanned Aerial Vehicles: State of the Art and the Road to Autonomy*, 1st ed., Springer, New York, 2007, pp. 171–210.

[6] Bouabdallah, S., Murrieri, P., and Siegwart, R., "Towards Autonomous Indoor Micro VTOL," *Autonomous Robots*, Vol. 18, No. 2, Mar 2005, pp. 171–183. doi:10.1007/s10514-005-0724-z

[7] Stepaniak, M. J., "A Quadrotor Sensor Platform," Ph.D. Dissertation, Russ College of Engineering and Technology, Ohio Univ., 2008.

[8] Stepaniak, M. J., Van Grass, F., and De Haag, M. U., "Design of an Electric Propulsion System for a Quadrotor Unmanned Aerial Vehicle," *Journal of Aircraft*, Vol. 46, No. 3, 2009, pp. 1050–1058. doi:10.2514/1.38409

[9] Pounds, P., and Mahony, R., "Design Principles of Large Quadrotors for Practical Applications," *IEEE International Conference on Robotics and Automation*, 2009, pp. 3265–3270. doi:10.1109/ROBOT.2009.5152390

[10] Pounds, P., Mahony, R., and Corke, P. I., "Design of a Static Thruster for Microair Vehicle Rotorcraft," *Journal of Aerospace Engineering*, Vol. 22, No. 1, 2009, pp. 85–94. doi:10.1061/(ASCE)0893-1321(2009)22:1(85)

[11] Pounds, P., Mahony, R., and Corke, P., "Modelling and Control of a Large Quadrotor Robot," *Control Engineering Practice*, Vol. 18, 2010, pp. 691–699. doi:10.1016/j.conengprac.2010.02.008

[12] Johnson, W., *Helicopter Theory*, 1st ed, Princeton Univ. Press, Princeton, IN, 1980, pp. 54, 338.

[13] Etkin, B., and Reid, L. D., "General Equations of Unsteady Motion," *Dynamics of Flight*, 3rd ed., Wiley, New York, 1996, pp. 95, 97, 101, 103.

[14] Lanzon, A., Feng, Y., Anderson, B. D. O., and Rotkowitz, M., "Computing the Positive Stabilizing Solution to Algebraic Riccati Equations with an Indefinite Quadratic Term via a Recursive Method," *IEEE Transactions on Automatic Control*, Vol. 53, No. 10, Nov. 2008, pp. 2280–2291. doi:10.1109/TAC.2008.2006108

[15] Zhou, K., Doyle, J. C., and Glover, K., *Robust and optimal control*, Prentice–Hall, Upper Saddle River, NJ, 1996, pp. 213–245.

[16] Isidori, A., Marconi, L., and Serrani, A., "Attitude Regulation of a LEO Rigid Satellite," *Robust Autonomous Guidance: An Internal Model Approach*, 1st ed, Springer, London, 2003, p. 229.

[17] Sidi, M. J., *Spacecraft Dynamics and Control, a Practical Engineering Approach*, 1st ed., Cambridge Univ. Press, Cambridge, England, U.K., 1997, pp. 6, 104, 152–160, 322, 327.

[18] Ducard, G. J. J., "Non Linear Control Design," *Fault-Tolerant Flight Control and Guidance Systems: Practical Methods for Small Vehicles*, 1st ed., Springer, London, 2009, pp. 107–120.

[19] Dehghani, A., Lanzon, A., and Anderson, B. D. O., "$H\infty$ Design to Generalize Internal Model Control," *Automatica*, Vol. 42, 2006, pp. 1959–1968. doi:10.1016/j.automatica.2006.06.007

[20] Lanzon, A., and Papageorgiou, G., "Distance Measure for Uncertain Linear Systems: A General Theory," *IEEE Transactions on Automatic Control*, Vol. 54, No. 7, July 2009, pp. 1532–1547. doi:10.1109/TAC.2009.2022098

[21] Pettazzi, L., Lanzon, A., Theil, S., and Ercoli Finzi, A., "Design of Robust Drag-Free Controllers with Given Structure," *Journal of Guidance, Control, and Dynamics*, Vol. 32, No. 5, Sept.–Oct. 2009, pp. 1609–1621. doi:10.2514/1.40279

[22] Lanzon, A., and Petersen, I. R., "Stability Robustness of a Feedback Interconnection of Systems with Negative Imaginary Frequency Response," *IEEE Transactions on Automatic Control*, Vol. 53, No. 4, May 2008, pp. 1042–1046. doi:10.1109/TAC.2008.919567

[23] Dehghani, A., Lecchini-Visintini, A., Lanzon, A., and Anderson, B. D. O., "Validating Controllers for Internal Stability Utilizing Closed-Loop Data," *IEEE Transactions on Automatic Control*, Vol. 54, No. 11, Nov. 2009, pp. 2719–2725. doi:10.1109/TAC.2009.2031587

[24] Lanzon, A., Lecchini, A., Dehghani, A., and Anderson, B. D. O., "Checking If Controllers are Stabilizing Using Closed-Loop Data," *45th IEEE Conference on Decision and Control*, 2006, pp. 3660–3665. doi:10.1109/CDC.2006.377549

[25] Kuipers, J. B., *Quaternions and Rotation Sequences: A Primer with Applications on Orbits, Aerospace, and Virtual Reality*, 1st ed., Princeton Univ. Press, Princeton, NJ, 1999, pp. 90, 108, 117, 264.